AUTHOR(S):

Sueno, Y; Honda, S; Kutsuma, H; Mima, S; Otani, C; Oguri, S; Suzuki, J; Tajima, O

京都大学学術情報リポジトリ
KURENAI 紅
Kyoto University Research Information Repository

京都大学
KYOTO UNIVERSITY

KURENAI 紅
Kyoto University Research Information Repository

Characterization of two-level system noise for a microwave kinetic inductance detector comprising niobium film on a silicon substrate

Y. Sueno[1,], S. Honda[2], H. Kutsuma[3], S. Mima[4], C. Otani[5], S. Oguri[6], J. Suzuki[1], and O. Tajima[1]

[1]*Department of Physics, Graduate School of Science, Kyoto University, Kitashirakawa-Oiwakecho, Sakyo-ku, Kyoto 606-8502, Japan*
[2]*Instituto de Astrofisica de Canarias, Calle Ví a Lá ctea, s/n, 38205 San Cristó bal de La Laguna, Santa Cruz de Tenerife, Spain*
[3]*RIKEN Center for Quantum Computing (RQC), RIKEN, 2-1 Hirosawa, Wako, Saitama, 351-0198, Japan*
[4]*Superconductive ICT Device Laboratory, Kobe Frontier Research Center, Advanced ICT Research Institute, National Institute of Information and Communications Technology, 588-2 Iwaoka, Nishi-ku, Kobe, Hyogo, 651-2492, Japan*
[5]*Terahertz Sensing and Imaging Research Team, RIKEN 519-1399 Aramaki-Aoba, Aoba-ku, Sendai, 980-0845, Miyagi, Japan*
[6]*Institute of Space and Astronautical Science (ISAS), Japan Aerospace Exploration Agency (JAXA) 3-1-1 Yoshinodai, Chuo-ku, Sagamihara, Kanagawa 252-5210, Japan*
E-mail: sueno.yoshinori.83x@st.kyoto-u.ac.jp

....
A microwave kinetic inductance detector (MKID) is a cutting-edge superconducting detector. It comprises a resonator circuit constructed with a superconducting film on a dielectric substrate. To expand its field of application, it is important to establish a method to suppress the two-level system (TLS) noise that is caused by the electric fluctuations between the two energy states at the surface of the substrate. The electric field density can be decreased by expanding the strip width (S) and gap width from the ground plane (W) in the MKID circuit, allowing the suppression of TLS noise. However, this effect has not yet been confirmed for MKIDs made with niobium films on silicon substrates. In this study, we demonstrate its effectiveness for such MKIDs. We expanded the dimension of the circuit from (S, W) = (3.00 μm, 4.00 μm) to (S, W) = (5.00 μm, 23.7 μm), and achieved an increased suppression of 5.5 dB in TLS noise.
....
Subject Index   H02, H20, H21, H22, H50

1. Introduction

A microwave kinetic inductance detector (MKID) is a cutting-edge superconducting detector [1,2]. Its readout scheme is based on natural frequency-domain multiplexing. This enables the reading of a large number of detector signals by using a pair of readout cables, each of $\mathcal{O}$(1000) pixels [3,4]. It thus enables the minimization of the heat load entering the detectors via cables. These advantages ensure that MKIDs are suitable for applications in radio astronomy [5–7].

For the radio detection, each MKID comprises an antenna-coupled superconducting resonator that is coupled to a feed line. As illustrated in Fig. 1, the resonator circuit and feed line are constructed using a coplanar waveguide (CPW) on a dielectric substrate. Resonances
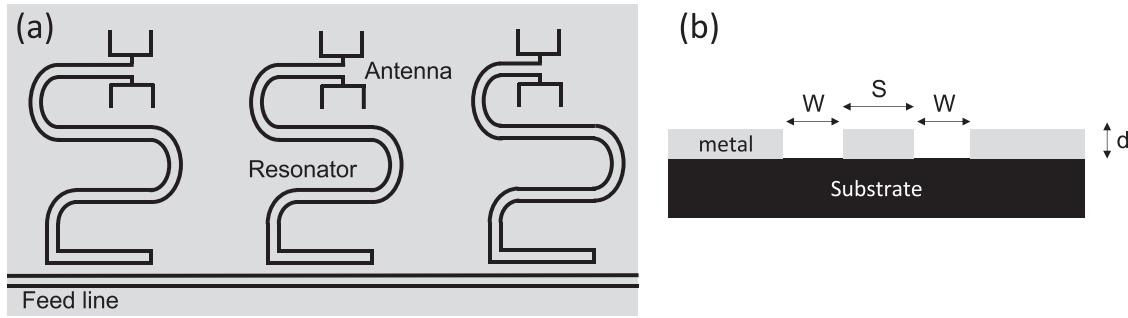
Fig. 1. (a) Schematic of the MKIDs. Each MKID comprises an antenna-coupled superconducting resonator that is coupled to the feed line. (b) Cross-sectional view of the CPW for the resonator film. In this study we define the center strip width, gap width, and thickness as S, W, and d, respectively.
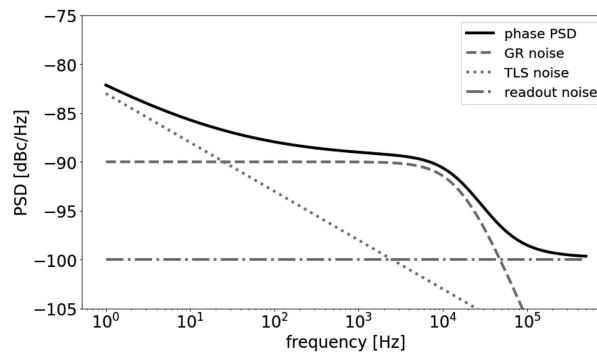

Fig. 2. Illustration of the typical MKID noise spectrum in the phase response. It consists of three noise components: GR noise, TLS noise, and readout noise.

of each MKID are monitored with the transmittance of the microwaves fed into the MKID. The radiation entering via the antenna breaks the Cooper pairs in the resonator film.[1] This is detected as a variation in the resonance, i.e. a variation in the resonant depth (known as amplitude response), and a variation in the resonant phase (known as phase response). The phase response is more commonly used because its responsivity is approximately one order of magnitude higher than that of the amplitude response [8,9].

The noise property of the MKID is usually characterized in a Fourier space. Fig. 2 illustrates the typical shape of a power spectrum density (PSD) in the phase response. There are three noise components: generation-recombination (GR) noise, two-level system (TLS) noise, and readout noise [10,11]. A source of GR noise is the generation and recombination of the quasiparticles in the resonator. Moreover, it is proportional to the number of quasiparticles, which depends on the physical temperature of the MKID and the critical temperature (T_c) of the film material, as well as the power of the input signals via the antenna. The mean time for recombination, known as the quasiparticle life time (τ_{qp}), is typically 10–1000 μs in the case of MKIDs made with an aluminum film. Therefore, there is no MKID response above this frequency, and the GR noise behaves as white noise below the frequency of $1/(2\pi\tau_{qp})$. The readout noise is dominated by the thermal noise of a cold low-noise amplifier (C-LNA) in the readout chain. This is generally maintained below the level of the GR noise. As described in the next section, the TLS noise is caused by electrical fluctuations at the surface of the substrate. This noise is

---

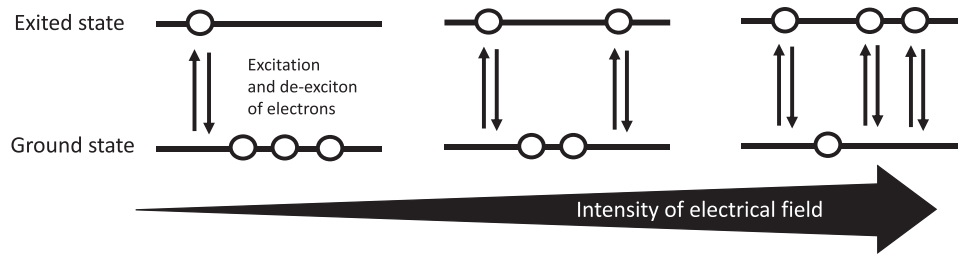[1]We phrase Cooper-pair breaking as quasiparticle generation.

Fig. 3. Mechanism of TLS fluctuation. The electrical field of the readout microwaves excites the energy states from the ground state to the excited state. De-excitation occurs over a finite length of time. These excitations and de-excitations are the origins of the electrical fluctuations. Therefore, the TLS noise depends on the frequency and power of the readout microwaves.

frequency dependent, and is of a higher magnitude in the lower-frequency region. Therefore, it is difficult to maintain low noise in the low-frequency region. Thus, the mitigation of TLS noise can enable the extension of low noise to the low-frequency region.

The magnitude of the TLS noise depends on the superconducting material at the resonator and the substrate material. Concerning the effect of substrate materials, a previous study demonstrated that an MKID using a silicon substrate achieved lower levels of TLS noise than an MKID using a sapphire substrate [12]. Similarly, studies conducted to assess the effect of superconducting materials demonstrated that aluminum generates higher levels of TLS noise than other materials [13].

However, aluminum ensures sensitivity to millimeter or sub-millimeter waves owing to its low gap energy that is necessary for Cooper-pair breaking. Therefore, minimizing the amount of aluminum used in the MKID circuit is a practical approach to mitigating the TLS noise, based on which a hybrid-type MKID [14] was designed. Its resonator comprises two different materials, and several combinations can be considered: niobium titanium nitride (NbTiN) and aluminum, titanium nitride (TiN) and aluminum, or niobium and aluminum. Although this hybrid-type MKID using NbTiN or TiN achieved good TLS noise suppression [15], the facilities that can use these materials are limited. Moreover, their fabrication is not simple [16]. Therefore, it is beneficial to develop a methodology of TLS noise reduction for niobium MKID.

Expanding the CPW geometry is another approach to suppressing the TLS noise [17]. To assess this approach, a study was conducted on MKIDs using niobium films on sapphire substrates [17]. However, there have been no published studies on MKIDs using niobium films on silicon substrates.

In this study we characterize the TLS noise for an MKID using a niobium film on a silicon substrate, and compare the magnitude of the TLS noise between two different CPW geometries. Our methods and results are presented as follows: In Sect. 2, we describe the properties of TLS noise. In Sect. 3, we describe the design and fabrication of the MKID devices. In Sect. 4, we characterize the TLS noise of these MKIDs. In Sect. 5, we discuss the difference in TLS noise between the two different CPW geometries. Finally, we state our conclusions in Sect. 6.

2. Two-level system noise
TLS noise is caused by electrical fluctuations between the ground state and an excited energy state at the surface of the substrate. The fluctuations between the two energy states are caused by readout microwaves that create electric fields at the surface of the CPW, as illustrated in Fig. 3.
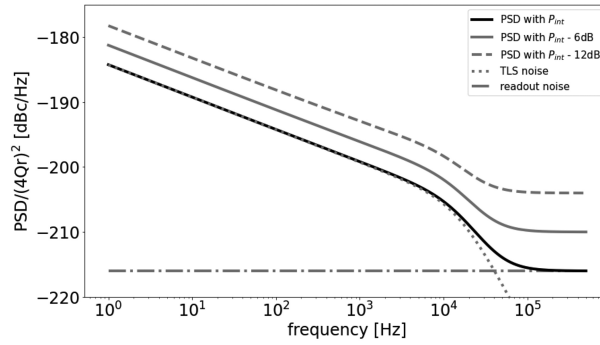
Fig. 4. Illustration of the expected PSDs for the MKID using niobium on the silicon substrate. The vertical axis is normalized by $(4Q_r)^2$ for the TLS noise study, as represented in Eq. (1). Here, we assume $Q_r = 10^5$. For the MKID fully made with the niobium film the GR noise is negligible because its T_c is high (9.2 K). The response speed of the readout microwaves in the resonator is described as the resonator ring time ($\tau_{res} = Q_r/\pi f_r$), which is typically 0.1–10 μs. There is no response to TLS fluctuation above the frequency $1/(2\pi\tau_{res})$.

As a result, fluctuations in the dielectric constant of the substrate cause fluctuations in the resonant frequency of the MKID. TLS noise can be characterized based on its dependence on three parameters. First, it has frequency dependence owing to the time intervals from excitation to de-excitation between the two energy states. Second, it has readout power dependence, which can be characterized by using the power law on the readout power.[2] Third, the TLS noise has temperature dependence. The occupancy of the excited states and the relaxation rate tend to be high when the device temperature is high [18]. Therefore, we obtain lower TLS noise at higher device temperatures.

We modeled the PSD for the TLS noise study based on the frequency (f), stored internal power in the resonator circuit (P_{int}), and device temperature (T),

$$PSD = (4Q_r)^2 \times N_{TLS} \left(\frac{f}{475\,\text{Hz}}\right)^{\alpha_f} \left(\frac{P_{int}}{-40\,\text{dBm}}\right)^{\alpha_P} \left(\frac{T}{0.33\,\text{K}}\right)^{\alpha_T}, \qquad (1)$$

where Q_r is a quality factor of the resonator; N_{TLS} represents the magnitude of the TLS noise; and α_f, α_P, and α_T are the power-law indices of frequency, internal power, and device temperature, respectively. P_{int} was calculated using the following formula according to Ref. [18]:

$$P_{int} = \frac{2Q_r^2}{\pi Q_c} P_{read}, \qquad (2)$$

where Q_c is a quality factor related to the coupling between the resonator and the feed line, and P_{read} is the power of the readout microwaves in the feed line. Then, we measured PSDs by changing the readout power as illustrated in Fig. 4. Following this, we extracted the model parameters N_{TLS}, α_f, and α_P from the measured PSDs. As discussed above, we expected negative values for α_f, α_P, and α_T. For the MKID made with the NbTiN film on a silicon substrate, these parameters were measured at $\alpha_f \approx -0.5$, $\alpha_P \approx -0.5$, and $\alpha_T \approx -2$, [19]; identical results were obtained for the MKID with niobium film on a sapphire substrate [21]. In this study, we assumed $\alpha_T = -2$ considering the limited cooling capacity.

N_{TLS} depends on the electric field density. We expected a lower electric field density with a wider CPW structure, as illustrated in Fig. 5. The concept we demonstrated in this study is that

---

[2]In general, a lower noise level is obtained with a higher readout power. However, the TLS fluctuation also depends on the readout power. We observe a combination of these in the PSD.
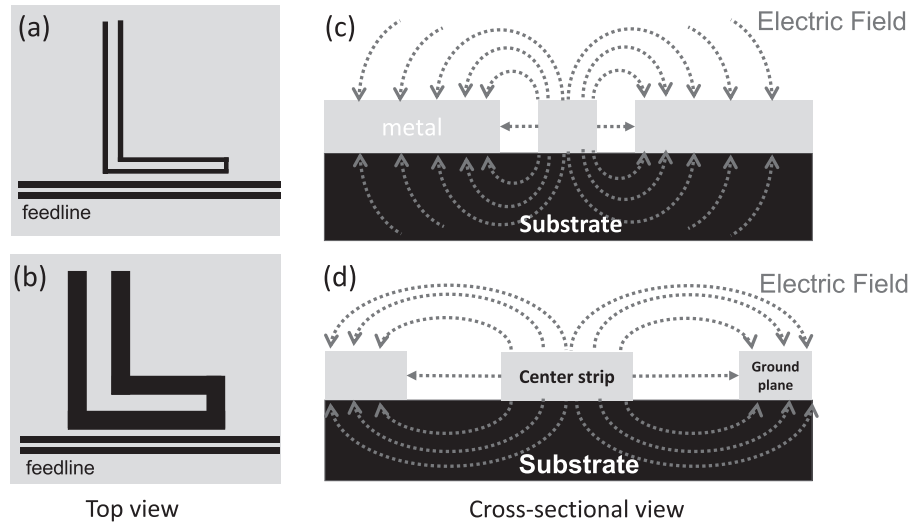
Fig. 5. The electric field density depends on the CPW geometry. Top and cross-sectional views of the CPW for MKIDs with narrow (a,c) and wide (b,d) geometries. The electric fields from the center strip line to the ground plane are illustrated in the cross-sectional views. The wide geometry has a lower electric field density than the narrow geometry.

Table 1. CPW parameters for the two types of MKID used in this study.

	Substrate	Film material	Film thickness (d)	Strip width (S)	Gap width (W)
Narrow-MKID	silicon	niobium	200 nm	3.00 μm	4.00 μm
Wide-MKID	silicon	niobium	200 nm	5.00 μm	23.7 μm

a lower N_{TLS} is obtained with a wider CPW structure. We expected to obtain approximately four times lower than N_{TLS} with a four times wider CPW structure.

3.   Design and fabrication of MKIDs

We fabricated two types of MKID, one with wide CPW geometry and the other with narrow CPW geometry. The main differences in their dimensions are the strip width and gap width in the CPW, as summarized in Table 1. The MKID with wide CPW geometry is denoted as "Wide-MKID" and the other as "Narrow-MKID." There have been simulation studies of the relations between the electric field density and CPW geometries [17,20], and they roughly obtained that the electric field density is inversely proportional to the strip width and gap width. With this knowledge, we expect that the electric field density of the Wide-MKID would be approximately 6 dB (i.e. four times) lower than that of the Narrow-MKID. Hence, the Wide-MKID generates lower TLS noise than the Narrow-MKID.

   The MKIDs used in this study were fabricated using equipment at RIKEN. They comprised a niobium film of 200 nm thickness on a ⟨100⟩-oriented Si wafer; their images are presented in Fig. 6. In the next section we characterize eight Wide-MKIDs and nine Narrow-MKIDs. We note that the MKIDs used in this study were designed specifically for the TLS noise study and are not hybrid-type MKIDs. They only use the niobium film as components, and thus the GR noise is negligible compared to the other two components— it is approximately two orders of magnitude lower than the readout noise.
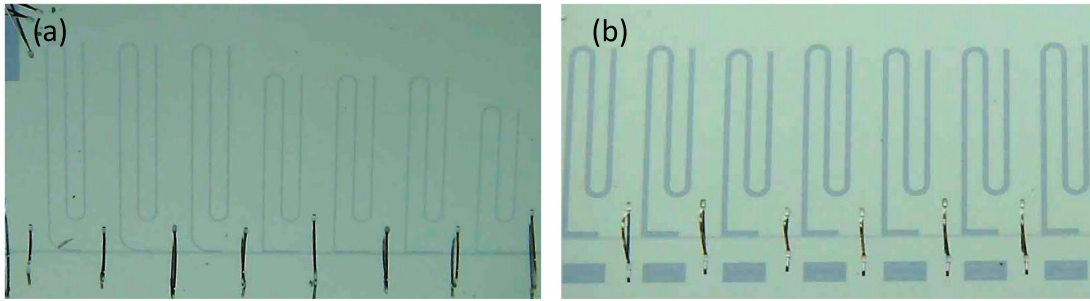
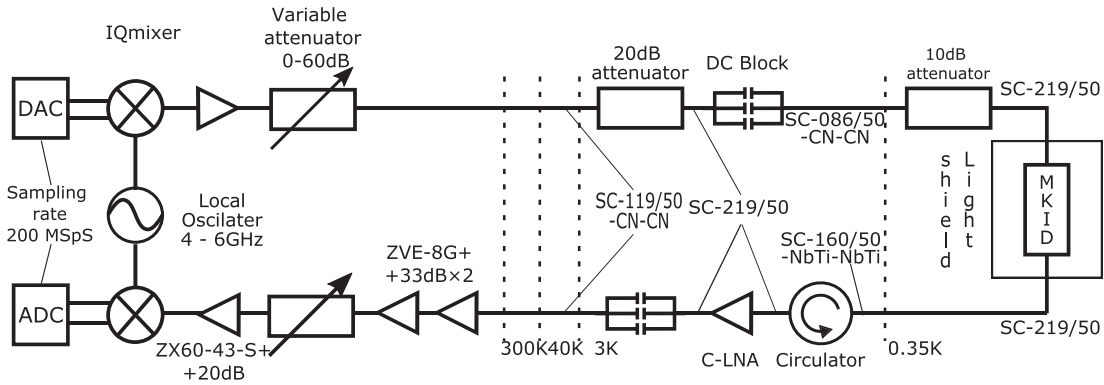**Fig. 6.** Images of (a) Narrow-MKID and (b) Wide-MKID.

Fig. 7. Diagram of the readout system. Readout microwaves (bandwidth of 200 MHz) were generated and sampled at a speed of 200 MHz [24]. The microwaves were up-converted and down-converted using an IQmixer (MLIQ-0218L, Marki Microwave) and a local oscillator (FSL-0010, NI Microwave Components). The readout power into the MKIDs was amplified with warm amplifiers (ZX60-83LN12+, Mini-Circuit) and tuned with variable attenuators. The readout power from the MKID was amplified with a cold low-noise amplifier (C-LNA, LNF-LN4_8C, LOWNOISE FACTORY), as well as warm amplifiers.

4.   Characterization of MKIDs

4.1.   *Cryostat and readout system*

We characterized the MKIDs at a temperature below 0.35 K. Our cryostat comprised a vacuum chamber, and first, second, and third radiation shields. The first and second shields were cryogenically cooled using a pulse tube refrigerator (PT407RM, Cryomech Co. Ltd) and maintained at 40 K and 3 K, respectively. Within the second shield, geomagnetism effects were maintained below 2 mG using magnetic shields (A4K, Amuneal Co. Ltd) set on the shield surface [22]. The third shield was a light-tight copper box, and was cooled using a ^{3}He-sorption refrigerator (Niki Glass Co. Ltd.), inside which we set the MKIDs. The Wide-MKIDs and Narrow-MKIDs were maintained at respective temperatures of 0.330 K and 0.348 K, and monitored with a 0.003 K accuracy.

A diagram of the readout circuit is shown in Fig. 7. The microwaves were generated using a digital-to-analog converter (DAC) with up-conversion using a mixer and a local oscillator (LO). Additionally, the microwave power at the insertion of the cryostat was adjusted from -19 dBm to -81 dBm using a variable attenuator (LDA-602, Vaunix Co. Ltd). With the attenuation of coaxial cables and attenuators set at 3 K and 0.35 K respectively, the microwave power into the MKID device (P_{read}) was reduced to the range -60 dBm to -122 dBm. The output microwaves from the MKID were amplified by 40 dB, with the C-LNA set to 3 K. To minimize
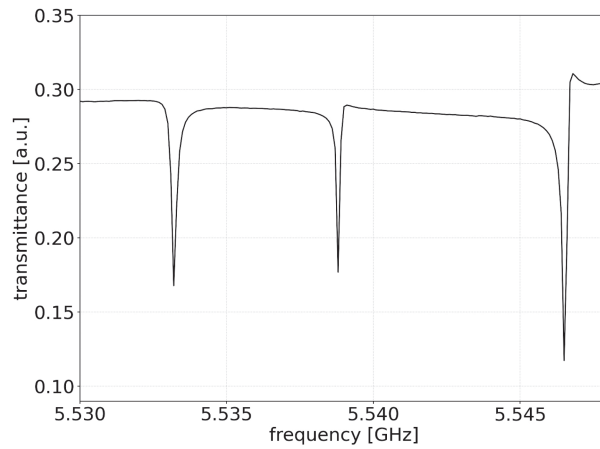
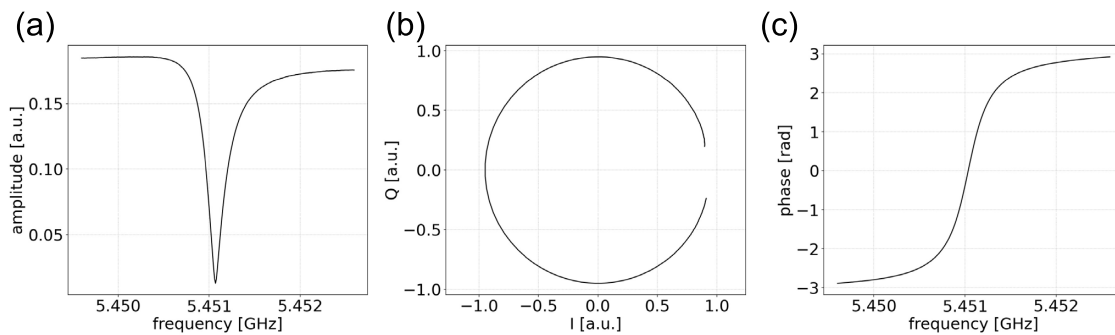**Fig. 8.** Transmittance of microwaves fed into the Wide-MKIDs.

Fig. 9. (a) Transmittance as a function of the frequency, (b) the resonant circle in the *I–Q* plane, and (c) the phase of the resonant circle of (b) for one MKID, W1.

thermal loading and the attenuation of microwaves we used a cable of superconducting material to connect the MKID device to the C-LNA. The output power of the microwaves from the cryostat was maintained in the range -31 dBm to -93 dBm, whereas the power entering the mixer was set to -11 dBm using the additional variable attenuator. Return microwaves were measured using an analog-to-digital converter (ADC) after down-conversion using the mixer and the LO. Two channels each of the DAC and ADC were employed, at a sampling rate of 200 MHz. For each frequency tone, the amplitude and phase responses were extracted based on direct down-conversion logic [23], and the down-sampled signals were recorded at a frequency below 1 MHz.

4.2. *Resonant frequencies and quality factors*

The resonant frequencies were identified based on the transmittance of the microwaves as a function of frequency, as shown in Fig. 8. For each resonance, the in-phase (*I*) and quadrature (*Q*) components were simultaneously measured, as shown in Fig. 9(b). Each resonance exhibits a similar circular response in the *I–Q* plane, and the MKID response is measured by the variation in the radius (amplitude) and phase. Q_r for each MKID is measured as the full width of the half minimum of the transmittance for each resonance. The radius of the resonant circle

Table 2. Resonant frequencies and quality factors for each MKID.

MKID	f_r [GHz]	Q_r [$\times 10^4$]	Q_c [$\times 10^4$]	Q_i [$\times 10^4$]
N1	4.00	10.8	12.7	68.9
N2	4.02	10.3	11.0	77.3
N3	4.03	7.32	9.15	27.2
N4	4.30	3.89	4.08	70.2
N5	4.32	3.92	4.17	63.2
N6	4.32	4.02	4.23	78.6
N7	4.59	1.29	1.28	77.0
N8	4.90	1.59	1.60	73.4
N9	4.92	1.64	1.55	81.0
W1	5.45	1.52	1.60	21.0
W2	5.48	3.42	3.77	24.1
W3	5.48	1.31	1.32	40.8
W4	5.49	2.82	3.81	8.57
W5	5.53	2.54	5.92	4.39
W6	5.54	5.87	10.5	12.8
W7	5.55	3.51	3.57	37.6
W8	5.59	1.29	1.35	19.0

represents the ratio Q_r/Q_c, and the internal quality factor (Q_i) is calculated using the formula

$$\frac{1}{Q_r} = \frac{1}{Q_i} + \frac{1}{Q_c}. \tag{3}$$

Q_i represents the energy stored in the resonator over its energy loss. The resonant frequencies and quality factors for each MKID, measured at $P_{read} = -90$ dBm, are summarized in Table 2. To facilitate comprehension, the Wide-MKIDs were labeled as W1, W2,..., W8, and the Narrow-MKIDs as N1, N2,..., N9. Notably, the radiation loss of the microwaves increases with the size of the CPW geometry (the details are described in Sect. 5). Hence, Q_i for the Wide-MKIDs is lower than for the Narrow-MKIDs.

4.3.　*Analysis of power spectrum density*

The time-ordered data (TOD) for each MKID were measured after identifying the resonant frequency, and three TODs were sampled for each MKID at every readout power condition: 100,000 samples with a 1 MHz sampling rate (i.e. a duration of 0.1 s), 100,000 samples with a 100 kHz sampling rate (i.e. a duration of 1 s), and 10,000 samples with a 1 kHz sampling rate (i.e. a duration of 10 s). The PSD was obtained as a function of the frequency by applying a fast Fourier transformation (FFT) for the three TODs. Fig. 10 presents the PSDs of the Narrow-MKID for three different P_{int} conditions. Here, the PSD was normalized by $(4Q_r)^2$ to characterize the TLS noise, as expressed in Eq. (1), and P_{int} dependence as well as frequency dependence was observed. This is consistent with the estimation in Fig. 4. Moreover, P_{int} was varied from -45 dBm to -30 dBm in 2 dBm steps.

The correlation of the TLS noise was characterized using P_{int} and the sampling frequency. As mentioned above, the contribution of the GR noise was negligible. Additionally, the contribution of the readout noise was removed from the final calculation. The readout noise was estimated as the averages of the high-frequency points (>474 kHz) in each PSD, from which it was subtracted.
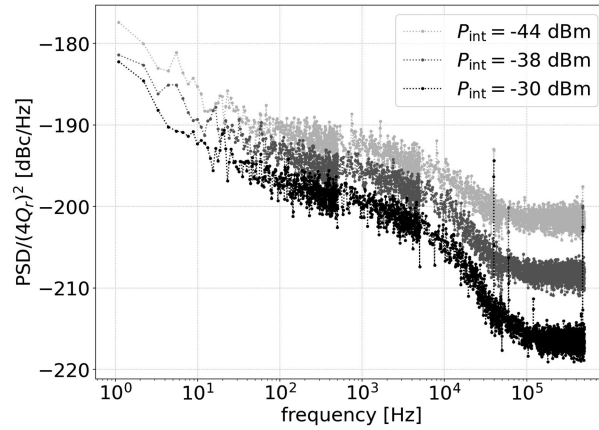
Fig. 10. Measured PSDs for the Narrow-MKID (N1) at three different P_{int} conditions. A reduction of the normalized PSD was observed while increasing P_{int}. As mentioned in Fig. 4, there was no response to TLS fluctuation in a short timescale below the resonator ring time ($\sim 10\,\mu$s). The readout noise ($>10^5$ Hz) is inversely proportional to the readout power. However, the reduction of the PSD in the lower-frequency region ($\leq 10^4$ Hz) is less significant owing to the P_{int} dependence of the TLS noise.
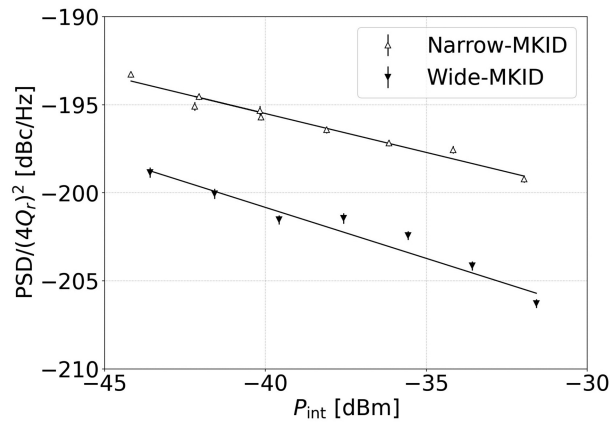

Fig. 11. Magnitude of the TLS noise as a function of P_{int}.

Fig. 11 presents the P_{int} dependence of the TLS noise for one of the Wide-MKIDs and one of the Narrow-MKIDs. Each data point is an average in the frequency range 450–500 Hz for each P_{int}. N_{TLS} and α_P were extracted by fitting using the formula in Eq. (1). The N_{TLS} and α_P values measured for each Narrow-MKID are summarized in Table 3, and the measurements for each Wide-MKID are summarized in Table 4. According to their averages, the Wide-MKIDs had approximately 5.7 dB lower N_{TLS} than the Narrow-MKIDs. All the α_P values that were obtained are consistent with our estimation, as discussed in Sect. 2. Additionally, they are also consistent with the values obtained in previous studies ($\alpha_P \approx -0.5$) [21].

To characterize the frequency dependence, averages in the five frequency regions were considered for the data collected under the condition $P_{\text{int}} = -40 \pm 1$ dBm: 90–100 Hz, 180–200 Hz, 450–500 Hz, 900–1000 Hz, and 1800–2000 Hz. The results are shown in Fig. 12. N_{TLS} and α_f were also extracted by fitting using Eq. (1). The values obtained are summarized in Tables 5 and 6 for the Narrow-MKIDs and Wide-MKIDs, respectively. Consequently, it was confirmed that the Wide-MKID has approximately 5.5 dB lower N_{TLS} than the Narrow-MKID, and that α_f is statistically consistent between the Wide-MKIDs and the Narrow-MKIDs. The overall

Table 3. Internal power dependence of TLS noise for the Narrow-MKIDs. For the average, the error was assigned as the standard deviation of each value.

	$N_{\mathrm{TLS}} + 200$ [dBc/Hz]	α_P [$\times\ 10^{-1}$]
N1	5.59 ± 0.05	-4.14 ± 0.12
N2	4.90 ± 0.06	-4.42 ± 0.17
N3	4.52 ± 0.06	-4.23 ± 0.13
N4	4.80 ± 0.06	-3.77 ± 0.12
N5	3.93 ± 0.07	-4.25 ± 0.13
N6	4.66 ± 0.07	-4.21 ± 0.16
N7	5.68 ± 0.10	-4.98 ± 0.19
N8	5.73 ± 0.09	-5.41 ± 0.21
N9	5.36 ± 0.10	-4.58 ± 0.22
Average	$5.06^{+0.56}_{-0.65}$	-4.44 ± 0.49

Table 4. Internal power dependence of TLS noise for the Wide-MKIDs. For the average, the error was assigned as the standard deviation of each value.

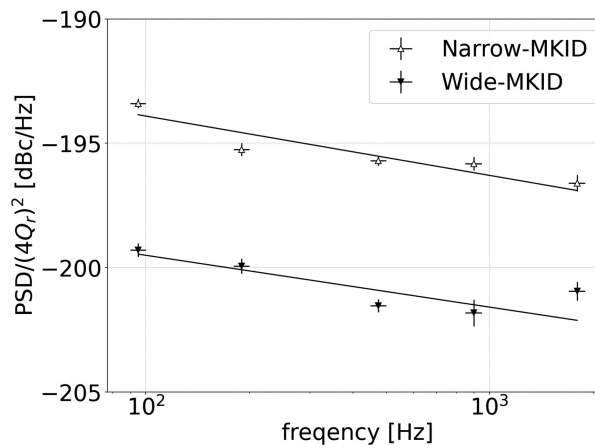|	$N_{\mathrm{TLS}} + 200$ [dBc/Hz]	α_P [$\times\ 10^{-1}$]
W1	$0.18^{+0.20}_{-0.21}$	-8.47 ± 0.62
W2	$-0.97^{+0.14}_{-0.15}$	-6.61 ± 0.26
W3	$-1.70^{+0.22}_{-0.24}$	-7.43 ± 0.78
W4	$-1.49^{+0.21}_{-0.22}$	-7.72 ± 0.90
W5	$-1.45^{+0.21}_{-0.22}$	-5.59 ± 0.68
W6	-1.22 ± 0.11	-4.17 ± 0.58
W7	-0.83 ± 0.12	-5.79 ± 0.59
W8	$1.33^{+0.24}_{-0.26}$	-5.20 ± 0.35
Average	$-0.65^{+1.03}_{-1.36}$	-6.37 ± 1.44

Fig. 12. Magnitude of the TLS noise as a function of frequency.

Table 5. Measured frequency dependence of TLS noise for the Narrow-MKIDs. For the average, the error was assigned as the standard deviation of each value.

MKID	$N_{TLS} + 200$ [dBc/Hz]	α_f [$\times 10^{-1}$]
N1	5.45 ± 0.08	-1.80 ± 0.49
N2	4.82 ± 0.10	-2.38 ± 0.61
N3	4.37 ± 0.10	-3.48 ± 0.80
N4	4.81 ± 0.11	-3.42 ± 1.19
N5	3.81 ± 0.11	-1.56 ± 0.63
N6	4.73 ± 0.10	-2.48 ± 0.31
N7	5.90 ± 0.12	-1.80 ± 1.19
N8	6.03 ± 0.12	-2.91 ± 0.80
N9	5.22 ± 0.13	-2.46 ± 0.38
Average	$5.07^{+0.66}_{-0.78}$	-2.46 ± 0.71

Table 6. Measured frequency dependence of TLS noise for the Wide-MKIDs. For the average, the error was assigned as the standard deviation of each value.

MKID	$N_{TLS} + 200$ [dBc/Hz]	α_f [$\times 10^{-1}$]
W1	$-0.09^{+0.31}_{-0.33}$	-2.54 ± 0.63
W2	$-1.08^{+0.20}_{-0.21}$	-1.30 ± 0.52
W3	$-1.01^{+0.23}_{-0.25}$	-1.35 ± 0.52
W4	$-0.00^{+0.21}_{-0.22}$	-1.79 ± 0.50
W5	$-0.58^{+0.28}_{-0.30}$	-2.93 ± 0.94
W6	-1.14 ± 0.18	-3.49 ± 0.54
W7	-0.72 ± 0.15	-2.08 ± 0.35
W8	$1.91^{+0.29}_{-0.31}$	-2.58 ± 0.71
Average	$-0.23^{+1.05}_{-1.38}$	-2.26 ± 0.77

average ($\alpha_f = -0.24 \pm 0.07$) is also consistent with that of previous studies ($\alpha_f \approx -0.5$), within its uncertainty (≈ 0.2) [19,21].

5.   Discussion

We successfully reduced TLS noise by employing a wide CPW geometry fabricated specifically for this study. The overall difference in N_{TLS} that we observed between the two types of MKID is approximately 5.5 dB, according to the naive averages from Tables 3–6. The uncertainty of Q_r in this measurement is below 2%, and it propagates to be 4% uncertainty for N_{TLS}. We interpret this improvement to result from the reduction in the electric field density at the CPW. As mentioned in Sect. 3, the magnitude of the electric field density for the Wide-MKID was predicted at approximately 6 dB lower than for the Narrow-MKID. As this estimation is close to the observed improvement for the N_{TLS}, it can be inferred that our results support the TLS noise mechanism described in Sect. 2.

However, despite reducing the TLS noise, the wide CPW geometry possesses a disadvantage: the wide gap in the resonator circuit causes radiation loss in the microwaves fed into it [25–27],

which degrades the internal quality factor,

$$\frac{1}{Q_i} = \frac{1}{Q_{i0}} + \frac{1}{Q_{loss}} + \frac{1}{Q_{load}}, \tag{4}$$

where Q_{i0}, Q_{loss}, and Q_{load} represent the quality factors that depend on the material, radiation loss, and external loading, respectively. In the laboratory measurement the external loading was negligible, and Q_i was limited by Q_{loss}. For the Wide-MKID (Narrow-MKID), we estimate $Q_{loss} \sim \mathcal{O}(10^4)$ ($\mathcal{O}(10^6)$) based on numerical simulation [25,28]. This estimation explains the differences in Q_i between the two types of MKID in Table 2. In the case of ground-based astronomical observations from the Earth, the effect of the radiation loss is negligible because external loading from the atmosphere is dominant. For example, to successfully demonstrate the negligible effect of radiation loss, we estimated $Q_{load} \sim 2 \times 10^4$ at the Teide Observatory in the Canary Islands in a frequency band of 150 GHz [29].

6. Conclusions

We studied TLS noise using two different types of MKID. The magnitude of the TLS noise for the MKID with wide CPW geometry was found to be 5.5 dB less than that with narrow CPW geometry, which was close to the expected reduction of 6 dB in the electric field density at the CPW. Additionally, the indices of the internal power and frequency dependence of the TLS noise are statistically consistent with those of previous studies. This is the first study to suppress the TLS noise by expanding the CPW geometry using MKIDs made with niobium film on a silicon substrate.

References

[1] P. K. Day, H. G. LeDuc, B. A. Mazin, A. Vayonakis, and J. Zmuidzinas, Nature **425**, 817 (2003).
[2] J. Zmuidzinas, Phys. Appl. **3**, 169 (2012).
[3] J. V. Rantwijk, M. Grim, D. V. Loon, S. Yates, A. Baryshev, and J. Baselmans, IEEE Trans. Microw. Theory Techn. **64**, 1876 (2016).
[4] J. J. A. Baselmans et al., Astron. Astrophys. **601**, A89 (2017).
[5] R. Adam et al., Astron. Astrophys. **609**, A115 (2018).
[6] K. Lee et al., Astrophys. J., **915**, 88 (2021).
[7] A. Endo et al., Nature Astron. **3**, 989 (2019).
[8] P. Visser, PhD thesis, TU Delft (2014).
[9] R. M. J. Janssen, J. J. A. Baselmans, A. Endo, L. Ferrari, S. J. C. Yates, A. M. Baryshev, and T. M. Klapwijk, Appl. Phys. Lett. **103**, 203503 (2013).
[10] W. A. Phillips, Rep. Prog. Phys. **50**, 1657 (1987).
[11] P. W. Anderson, B. I. Halperin, and C. M. Varma, Philos. Mag. **25**, 1 (1972).
[12] R. Barends, H. L. Hortensius, T. Zijlstra, J. J. A. Baselmans, S. J. C. Yates, J. R. Gao, and T. M. Klapwijk, IEEE Trans. Appl. Supercond. **19**, 936 (2009).
[13] J. Gao and J. Zmuidzinas, Appl. Phys. Lett. **90**, 102507 (2007).
[14] S. J. C. Yates, J. J. A. Baselmans, A. Endo, R. M. J. Janssen, L. Ferrari, P. Diener, and A. M. Baryshev, Appl. Phys. Lett. **99**, 073505 (2011).
[15] R. Barends, H. L. Hortensius, T. Zijlstra, J. J. A. Baselmans, S. J. C. Yates, J. R. Gao, and T. M. Klapwijk, IEEE Trans. Appl. Supercond. **19**, 936 (2009).

[16] B. G. C. Bos, D. J. Thoen, E. A. F. Haalebos, P. M. L. Gimbel, T. M. Klapwijk, J. J. A. Baselmans, and A. Endo, IEEE Trans. Appl. Supercond. **27**, 1500405 (2017).
[17] J. Gao et al., Appl. Phys. Lett. **92**, 212504 (2008).
[18] S. Kumar, J. Gao, J. Zmuidzinas, B. A. Mazin, H. G. LeDuc, and P. K. Day, Appl. Phys. Lett. **92**, 123503 (2008).
[19] R. Barends, N. Vercruyssen, A. Endo, P. J. de Visser, T. Zijlstra, T. M. Klapwijk, and J. J. A. Baselmans, Appl. Phys. Lett. **97**, 033507 (2010).
[20] H. Wang et al. Appl. Phys. Lett. **95**, 233508 (2009).
[21] J. Gao, PhD thesis, California Institute of Technology (2008).
[22] H. Kutsuma, M. Hattori, K. Kiuchi, S. Mima, T. Nagasaki, S. Oguri, J. Suzuki, and O. Tajima, J. Low Temp. Phys. **193**, 203 (2018).
[23] J. Suzuki, H. Ishitsuka, K. Lee, S. Oguri, O. Tajima, N. Tomita, and E. Won, J. Low Temp. Phys. **193**, 562 (2018).
[24] H. Ishitsuka, M. Ikeno, S. Oguri, O. Tajima, N. Tomita, and T. Uchida, J. Low Temp. Phys. **184**, 424 (2016).
[25] S. Hähnle, N. v. Marrewijk, A. Endo, K. Karatsu, D. J. Thoen, V. Murugesan, and J. J. A. Baselmans, Appl. Phys. Lett. **116**, 182601 (2020).
[26] J. Zmuidzinas, Ann. Rev. Cond. Matt. Phys. **3**, 169 (2012).
[27] B. A. Mazin, PhD thesis, California Institute of Technology (2004).
[28] J. M. Sage et al., J. Appl. Phys. **109**, 063915 (2011).
[29] H. Kutsuma, PhD thesis, Tohoku University (2021).